Partial volume effect correction impairs the diagnostic utility of [18F]-THK-5351 PET in nonfluent-agrammatic variant primary progressive aphasia

Patrick J. Sommer, Sebastian Schuster, Oliver Goldhardt, Nobuyuki Okamura, Felix Mueller-Sarnowski, Maximilian Scheifele, Florian Eckenweber, Annika Kreuzer, Maria Griessl, Peter Bartenstein, Thomas Wegehaupt, Lucas Wolski, Josef Priller, Axel Rominger, Leonie Beyer, Timo Grimmer, Matthias Brendel

Angaben zur Veröffentlichung / Publication details:

Sommer, Patrick J., Sebastian Schuster, Oliver Goldhardt, Nobuyuki Okamura, Felix Mueller-Sarnowski, Maximilian Scheifele, Florian Eckenweber, et al. 2025. "Partial volume effect correction impairs the diagnostic utility of [18F]-THK-5351 PET in nonfluent-agrammatic variant primary progressive aphasia." NeuroImage: Clinical 46: 103789. https://doi.org/10.1016/j.nicl.2025.103789.

NeuroImage: Clinical 46 (2025) 103789

Contents lists available at ScienceDirect

NeuroImage: Clinical

journal homepage: www.elsevier.com/locate/ynicl

Partial volume effect correction impairs the diagnostic utility of [^{18}F]-THK-5351 PET in nonfluent-agrammatic variant primary progressive aphasia

Patrick J. Sommer [a,*,1], Sebastian Schuster [b,c,1], Oliver Goldhardt [a], Nobuyuki Okamura [d,e], Felix Mueller-Sarnowski [a,f], Maximilian Scheifele [b], Florian Eckenweber [b], Annika Kreuzer [b], Maria Griessl [b], Peter Bartenstein [b], Thomas Wegehaupt [a], Lucas Wolski [a], Josef Priller [a,g,h,i], Axel Rominger [j], Leonie Beyer [b], Timo Grimmer [a,2], Matthias Brendel [b,k,l,2]

[a] Center for Cognitive Disorders, Department of Psychiatry and Psychotherapy, Technical University of Munich, School of Medicine and Health, TUM University Hospital, Munich, Germany
[b] Department of Nuclear Medicine, Ludwig-Maximilian-University Munich, Munich, Germany
[c] Institute of Diagnostic and Interventional Radiology and Neuroradiology, Munich Clinic Harlaching, Munich, Germany
[d] Division of Pharmacology, Faculty of Medicine, Tohoku Medical and Pharmaceutical University, Sendai, Japan
[e] Division of Brain Science, Department of Aging Research and Geriatric Medicine, Institute of Development, Aging, and Cancer, Tohoku University, Sendai, Japan
[f] Department of Medical Information Science, School of Medicine, Augsburg University, Augsburg, Germany
[g] German Center for Neurodegenerative Diseases (DZNE), Berlin, Germany
[h] Department of Psychiatry and Psychotherapy, Charité, Berlin, Germany
[i] Centre for Clinical Brain Sciences, University of Edinburgh and UK DRI, Edinburgh, UK
[j] Department of Nuclear Medicine, Inselspital Bern, University of Bern, Bern, Switzerland
[k] German Center for Neurodegenerative Diseases (DZNE), Munich, Germany
[l] Munich Cluster of Systems Neurology (SyNergy), Munich, Germany

ARTICLE INFO

Keywords:
Primary progressive aphasia
Positron-emission-tomography
[^{18}F]-THK-5351
Partial volume effect
tau-PET
Cortical atrophy

ABSTRACT

Objectives: Partial volume effects in positron emission tomography occur frequently in neurodegenerative diseases due to increasing cortical atrophy during the disease course, and fronto-temporal dementia is often characterized by severe atrophy. The aim of this study was to challenge partial volume effect correction (PVEC) in patients with nonfluent-agrammatic variant primary progressive aphasia (nfv-PPA) imaged with [^{18}F]-THK-5351 PET a marker of reactive neuroinflammatory astrogliosis as well as tau-binding.

Methods: Patients with nfv-PPA (n = 20) were imaged with [^{18}F]-THK-5351 PET accompanied by structural magnetic resonance tomography imaging (MRI). Region specific cortical grey matter volumes and standard uptake value ratios (SUVr) of the Hammers atlas were compared with eight healthy control (HC) (n = 8) data before and after performing region-based voxel-wise PVEC. We evaluated regional coefficients of variance (CoV) and the number of regions with significant [^{18}F]-THK-5351 PET signal differences between nfv-PPA and controls before and after PVEC. Additionally, a blinded visual read was performed by three nuclear medicine physicians (consensus) before and after PVEC.

Results: Prior to PVEC, [^{18}F]-THK-5351 tracer uptake was significantly higher in the bilateral frontal cortex of patients with nfv-PPA when compared to HC (left > right), despite significant grey matter atrophy in the same brain regions in patients with nfv-PPA. SUVr differences between nfv-PPA and HC were further increased by PVEC in frontal brain regions, but group level variance increased in parallel and reduced the number of significant differences between SUVr of nfv-PPA and HC (uncorrected: 10 significant regions, CoV[nfv-PPA]: 20.8 % ± 4.7 %, CoV[HC]: 7.9 % ± 2.4 %/PVEC: 3 significant regions, CoV[nfv-PPA]: 28.4 % ± 8.9 %, CoV[HC]: 9.8 % ± 2.5 %). Sensitivity/specificity of the visual read for detection of nfv-PPA was 0.85/1.00 without PVEC and 0.85/0.75 with PVEC.

* Corresponding author.
E-mail address: Patrick.Sommer@tum.de (P.J. Sommer).
[1] Shared first authorship.
[2] Contributed equally.

https://doi.org/10.1016/j.nicl.2025.103789
Received 12 August 2024; Received in revised form 22 February 2025; Accepted 15 April 2025
Available online 24 April 2025

Conclusions: [^{18}F]-THK-5351 PET facilitates detection of pathological alterations in patients with nfvPPA with severe atrophy. PVEC increases quantitative SUVr differences between patients with nfv-PPA and HC but introduces a parallel increase of variance at the group level. Visual assessment of [^{18}F]-THK-5351 images in patients with nfv-PPA is impaired by PVEC due to loss of specificity and does not support the use of PVEC even in patients with severe atrophy.

1. Introduction

Primary progressive aphasia (**PPA**) comprises a group of different clinicopathological syndromes from the spectrum of frontotemporal lobar degeneration (**FTLD**) characterized by speech and language impairments (Gorno-Tempini et al., 2011; Ruksenaite et al., 2021). Depending on the predominant symptoms PPAs are further subdivided into three major variants: the semantic-variant PPA (**sv-PPA**) with impaired single-word comprehension, the nonfluent/agrammatic variant PPA (**nfv-PPA**) with agrammatism and speech apraxia, and the logopenic-variant PPA (**lv-PPA)** with impaired single-word retrieval as its major clinical feature (Spinelli et al., 2017).

The cause of PPA is assumed to be the spread of an underlying proteinopathy within neuronal language networks (Ruksenaite et al., 2021; Mesulam et al., 2014). Even though each PPA variant can originate from a variety of possible underlying proteinopathies, it must be noted, that each distinct PPA variant is disproportionately caused by one preferred proteinopathy. While mostly all patients with lv-PPA show Alzheimer's disease (AD) pathology and the majority of sv-PPA patients indicate Transactive response DNA binding protein 43 (TDP-43) proteinopathy as the underlying pathology, tau-pathology has been found to be the leading cause of disease in a predominant proportion (75–100 %) of nfv-PPA patients (Hodges et al., 2004; Mackenzie and Neumann, 2016; Josephs et al., 2006; Mesulam et al., 2014; Harris et al., 2013).

Having tau-pathology as the most likely underlying proteinopathy, nfv-PPA patients represent an interesting cohort for positron-emission-tomography (PET) with radiotracers aiming to detect tau (Josephs et al., 2018). Different first-generation tau radiotracers ([^{18}F]-flortaucipir, [^{18}F]-THK-5351) illustrated characteristic binding patterns in all three subtypes with spatial overlap to regions with morphological atrophy also in tau-negative sv-PPA (Josephs et al., 2018; Yoon et al., 2018; Cho et al., 2019; Makaretz et al., 2018). Due to the known off-target binding to MAO-A/B in first-generation tau radiotracers, the resulting tracer signal is thought to derive from both tau-specific and off-target binding due to reactive neuroinflammatory astrogliosis-related MAO-B elevation in affected brain regions (Ng et al., 2017; Harada et al., 2018; Vermeiren et al., 2018). The diagnostic value of such a combined reactive neuroinflammatory astrogliosis/tau radiotracer for differentiating different neurodegenerative entities has previously been proven for parkinsonian syndromes and clinical diagnostic utility seems likely also in PPA (Josephs et al., 2018; Schönecker et al., 2019; Schaeverbeke et al., 2018; Brendel et al., 2018; Brendel et al., 2017).

In nfv-PPA, only small sample sizes (n = 13, n = 12, n = 3) have been investigated so far with two different first-generation radiotracers, [^{18}F]-flortaucipir and [^{18}F]-THK-5351 (Josephs et al., 2018; Yoon et al., 2018; Schaeverbeke et al., 2018). Studies using [^{18}F]-THK-5351 as tracer reported an elevated radiotracer signal pronounced in the bilateral frontal cortex, matching the predicted anatomical distribution of tau-pathology (Yoon et al., 2018; Schaeverbeke et al., 2018). As PET imaging in neurodegenerative diseases is known to suffer from partial volume effects (PVE) due to cortical atrophy, the diagnostic accuracy of different radiotracers can be hampered by the limited spatial resolution of the scanner (Thomas et al., 2011). Many previous preclinical and clinical studies with different radiotracers proposed partial volume effect correction (PVEC) to increase the tracer signal and thereby reveal the real amount of underlying pathology (Thomas et al., 2011; Brendel et al., 2014; Brendel et al., 2015; Brendel et al., 2016). For [^{18}F]-THK-5351, different PVEC algorithms were tested in hippocampal regions of AD and healthy controls (HC) and uncorrected standard uptake value ratios (SUVRs) were underestimated for all PVEC approaches (Oyama et al., 2020). In a combined study with PET and magnetic resonance imaging (MRI) in AD patients, the tracer retention patterns were found to be similar before and after PVEC.

As severe atrophy of the frontal and temporal cortex is one essential feature of FTLD, PVEC could be of high importance especially in nfv-PPA patients (Lombardi et al., 2021). In the only study using PVEC in all PPA patients, scans with and without PVEC revealed similar results (Schaeverbeke et al., 2018). However, so far there has not been a study that systematically challenged the diagnostic utility of PVEC in nfv-PPA patients.

The aim of this study therefore was to investigate the utility of PVEC in nfv-PPA patients undergoing [^{18}F]-THK-5351-PET imaging.

2. Material and methods

2.1. Clinical evaluation

Twenty nfv-PPA patients (age: 62.8 ± 11.4 years, 9 male) from the Technical University of Munich's Centre for Cognitive Disorders, an outpatient clinic at the Department of Psychiatry, Technical University of Munich (TUM), were enrolled in the study and referred to [^{18}F]-THK-5351-PET imaging at the Department of Nuclear Medicine, LMU Munich. Diagnosis was made according to the diagnostic criteria for nfv-PPA of Gorno-Tempini (Gorno-Tempini et al., 2011). The cognitive abilities were assessed by Mini-Mental Stat examination (MMSE) and Clinical Dementia Rating Scale (CDR). Each test or examination was performed by a trained neuropsychologist. For calculation of disease duration time the time between disease onset and imaging date was used. A previously published healthy control (HC) cohort was used for quantitative comparison of PET signals between diseased and healthy brain. The HC cohort was sex matched but not age matched (n = 8, age: 71.7 ± 6.7 years, 4 male) and harmonized to the scanner that was used for patient imaging (Brendel et al., 2017); one previously published control was excluded because MRI quality was not sufficient to perform PVEC. Written informed consent for [^{18}F]-THK-5351-PET imaging was obtained by all participants in accordance with the Declaration of Helsinki. Retrospective analysis of data had been approved by the local ethics committee (Ethics approval Nr. 444–16).

2.2. [^{18}F]-THK-5351-PET & MRI quantification and visual analysis

Automated production of [^{18}F]THK-5351 was performed on a Raytest® SynChrom R&D single reactor synthesizer as reported previously and all emission recordings were performed in a previously established procedure (Schönecker et al., 2019; Brendel et al., 2017). Dynamic three-dimensional emission recordings were required from 50-70 min after injection of 188 ± 18 MBq [^{18}F]-THK-5351 using a GE Discovery 690 PET/CT scanner with a low-dose CT scan for attenuation correction.

Anatomical MRI was performed using a Philips Ingenia Elition X. 3 Tesla Scanner with the Software Version 5.6. in nfv-PPA patients and a Signa 1.5 Tesla machine (General Electric) in control subjects as described previously (Brendel et al., 2017).

The PNEURO (V3.9 Zurich, Switzerland) pipeline was used to analyze all PET and MRI scans as described previously (Schuster et al., 2022). In brief, individual T1-weighted MR images were used to

Table 1
Demographics of the two study groups. nfv-PPA = nonfluent variant primary progressive aphasia, SD = standard deviation, CDR = Clinical Dementia Rating scale, MMSE = Mini-Mental State examination.

	Nfv-PPA	Healthy controls (HC)	P −Value
Numbers (n)	20	8	–
Sex: male:female (%)	9: 11 (45 %: 55 %)	4:4 (50 %:50 %)	0.810595
Age: in years			
Mean ± SD (min–max)	62.8 ± 11.4 (50—83)	71.7 ± 6.7 (61—81)	0.0499
Median (1st; 3rd quartile)	63.0 (57.3; 71.8)	71.0 (67.0; 80.0)	–
Education: in years			
Mean ± SD (min–max)	14.7 ± 4.1 (9—23)	–	–
Median (1st; 3rd quartile)	13 (12; 18)	–	–
Disease Duration: in months			
Mean ± SD (min–max)	18.9 ± 10.6 (4—37)	–	–
Median (1st; 3rd quartile)	15.0 (9.8; 27.0)	–	–
CDR global:			
Mean ± SD (min–max)	0.7 ± 0.3 (0—1)	–	–
Median (1st; 3rd quartile)	0.5 (0.5; 1.0)	–	–
MMSE:			
Mean ± SD (min–max)	23.0 ± 6.2 (11—30)	–	–
Median (1st; 3rd quartile)	25.5 (21.3; 27.3)	–	–

segment the brain into non-overlapping regions of interest (ROIs) for region-based voxel-wise correction as described previously including the following steps: (i) parcellation consisting of probability masks for n anatomical structures, (ii) GTM algorithm for corrected values of T, (iii) voxel-wise correction (Thomas et al., 2011).

For semiquantitative analyses, (i) grey matter volumes (ii) mean standard-uptake-value ratios (SUVr) relative to the cerebellar grey matter of uncorrected volumes of interest (VOIs) and (iii) mean SUVr relative to the cerebellar grey matter of uncorrected VOIs were extracted for all lobes (detailed Hammers atlas regions for the frontal and temporal lobe) in all subjects.

Three expert readers independently assessed the [^{18}F]-THK-5351 maps in 3D mode using standardized settings (lower/upper SUVr threshold 1.0/3.0; rainbow color, overlay on a MRI standard template in the MNI space with 50 % transparency) as presented by the PMOD viewer and blinded to the identity of the subject. Each reader had to score the overall pattern of the scan as positive or negative for a nfv-PPA-typical [^{18}F]-THK-5351 binding pattern. In particular, the reader was instructed to evaluate binding in the frontal and temporal cortex together with the adjacent subcortical white matter structures and the final decision of positivity or negativity of a nfvPPA-typical pattern was dichotomous for the entire scan. The majority judgment from the three readers defined positivity and negativity for a nfv-PPA-like [^{18}F]-THK-5351 PET scan. Fleiss κ was determined as a measure of intra-reader agreement. Furthermore, each reader rated the subjective level of confidence for all evaluated images with a five item scale (very low, low, intermediate, high, very.high).

2.3. Statistical analysis

GraphPad Prism (version 8.4.3, GraphPad Software Inc., San Diego, CA, USA), Excel (Microsoft, Redmond, USA), SPSS (IBM, Ehningen, Germany) and R version 4.3.2 (R Core Team, 2023).

was used for statistical analysis and illustration of results. Demographics were compared using $\chi 2$ – test for sex and T-test for age distribution. Grey matter volumes and uncorrected/corrected [^{18}F]-THK-5351 SUVr for all cortical regions were compared group-wise between nfv-PPA patients and HC using Mann-Whitney tests with subsequent Benjamini-Hochberg correction for multiple testing (Benjamini and Hochberg, 1995).

Table 2
Grey matter volumes of predefined brain regions in both study groups. Significant p-values for the grey matter volume difference between patients with nonfluent variant primary progressive aphasia (nfv-PPA) and healthy controls (HC) are highlighted in bold; SD = standard deviation; p_{cor} −value = p-value corrected for multiple testing.

Cortical region	Mean volume left ± SD (ccm^3)			Mean volume right ± SD (ccm^3)		
	HC	nfv-PPA	p_{cor}-value	HC	nfv-PPA	p_{Cor}-value
Precentral gyrus (FL_precen)	17.4 ± 0.9	17.8 ± 1.6	0.573	16.9 ± 1.1	17.9 ± 1.4	0.210
Superior frontal gyrus (FL_sup_fr)	34.9 ± 1.9	30.7 ± 3.7	**0.013**	35.9 ± 1.5	31.9 ± 3.2	**0.008**
Middle frontal gryus (FL_mid_fr)	30.5 ± 1.0	26.9 ± 3.2	**0.008**	31.1 ± 1.0	28.8 ± 2.7	0.071
Inferior frontal gyrus (FL_inf_fr)	13.1 ± 1.0	12.2 ± 1.3	0.198	12.1 ± 0.9	12.0 ± 0.8	0.916
Straight gyrus (FL_strai)	3.5 ± 0.2	3.1 ± 0.4	**0.009**	3.9 ± 0.3	3.5 ± 0.3	**0.009**
Anterior cingulate gyrus (G_cing_ant)	7.8 ± 0.4	6.2 ± 0.8	**0.004**	7.4 ± 0.4	6.5 ± 0.6	**0.006**
Anterior orbital gyrus (FL_OFC_AOG)	5.1 ± 0.4	4.4 ± 0.4	**0.003**	5.0 ± 0.3	4.4 ± 0.4	**0.003**
Medial orbital gyrus (FL_OFC_MOG)	5.2 ± 0.3	4.7 ± 0.4	**0.014**	4.9 ± 0.3	4.6 ± 0.4	0.092
Lateral orbital gyrus (FL_OFC_LOG)	2.8 ± 0.2	2.5 ± 0.2	**0.013**	3.2 ± 0.2	2.8 ± 0.2	**0.002**
Posterior orbital gyrus (FL_OFC_POG)	4.0 ± 0.4	4.1 ± 0.3	0.254	4.0 ± 0.3	4.0 ± 0.3	>0.999
Anterior medial temporal gyrus (Ant_TL_med)	6.3 ± 0.4	5.8 ± 0.6	0.079	6.1 ± 1.1	6.2 ± 0.5	0.690
Anterior inferior lateral temporal gyrus (Ant_TL_inf_lat)	3.1 ± 0.2	2.6 ± 0.4	**0.003**	3.4 ± 0.3	2.9 ± 0.3	**0.008**
Parahippocampal and ambient gyrus (G_paraH_amb)	4.7 ± 0.1	4.6 ± 0.3	0.681	4.5 ± 0.2	4.4 ± 0.3	>0.999
Superior posterior temporal gyrus (G_sup_temp_post)	9.7 ± 0.6	9.5 ± 0.8	0.677	10.0 ± 0.8	4.0 ± 0.8	0.997
Middle and inferior temporal gyrus (G_tem_midin)	13.3 ± 0.7	13.1 ± 1.0	0.956	13.5 ± 0.8	14.0 ± 0.9	0.577
Fusiforme gyrus (G_fus)	4.6 ± 0.2	4.2 ± 0.5	0.135	4.4 ± 0.1	4.4 ± 0.2	0.806
Posterior temporal gyrus (Post_TL)	35.0 ± 1.6	33.7 ± 2.0	0.319	35.9 ± 1.8	36.0 ± 1.9	>0.999
Superior anterior temporal gyrus (G_sup_temp_ant)	4.0 ± 0.4	3.7 ± 0.4	0.282	3.7 ± 0.4	4.0 ± 0.4	>0.999
Parietal lobe (PL_rest)	28.2 ± 1.8	25.8 ± 2.1	**0.018**	28.1 ± 1.4	27.0 ± 1.6	0.201
Occipital lobe (OL_rest_lat)	31.5 ± 1.6	31.5 ± 2.1	0.980	32.3 ± 1.4	32.6 ± 1.7	0.721

3. Results

3.1. Demographics and clinical data

The range of age was between 51 and 83 years with years of education lasting from 9 to 23, a disease duration up to 3 years, and MMSE scores between 11 and 30.

Detailed demographics and neuropsychological data of patients and of healthy controls are listed in Table 1.

Table 3
Differences of [^{18}F]-THK-5351 binding between patients with nonfluent variant primary progressive aphasia (nfv-PPA) and healthy controls (HC) in both hemispheres using predefined brain regions with and without partial volume effect correction (PVEC). Significant p-values are highlighted in bold; PVEC = partial volume effect, SUVr = standard uptake value ratio, SD = standard deviation, CoV = Coefficient of variation, p_{cor} −value = p-value corrected for multiple testing.

Cortical region	Mean SUVr left ± SDwithout PVEC					Mean SUVr right ± SDwithout PVEC					Mean SUVr left ± SDwith PVEC					Mean SUVr right ± SDwith PVEC				
	HC	CoV_{HC}	nfv-PPA	CoV_{NV}	$_{PCor}$-value	HC	CoV_{HC}	nfv-PPA	CoV_{NV}	$_{PCor}$-value	HC	CoV_{HC}	nfv-PPA	CoV_{NV}	$_{PCor}$-value	HC	CoV_{HC}	nfv-PPA	CoV_{NV}	$_{PCor}$-value
Precentral gyrus (FL_precen)	1.12 ± 0.07	0.063	1.39 ± 0.40	0.291	0.074	1.12 ± 0.0,07	0.068	1.23 ± 0.28	0.228	0.690	1.04 ± 0.11	0.108	1.48 ± 0.68	0.460	0.066	1.05 ± 0.14	0.128	1.27 ± 0.44	0.350	0.348
Superior frontal gyrus (FL_sup_fr)	**1.28 ± 0.10**	**0.084**	**1.65 ± 0.39**	**0.233**	**0.034**	1.30 ± 0.10	0.083	1.52 ± 0.32	0.208	0.156	1.41 ± 0.15	0.106	1.94 ± 0.62	0.322	0.068	1.44 ± 0.15	0.102	1.75 ± 0.46	0.261	0.134
Middle frontal gryus (FL_mid_fr)	**1.26 ± 0.08**	**0.068**	**1.71 ± 0.38**	**0.224**	**0.032**	1.24 ± 0.08	0.068	1.53 ± 0.36	0.236	0.074	1.35 ± 0.13	0.092	1.99 ± 0.64	0.323	0.076	1.32 ± 0.12	0.094	1.75 ± 0.58	0.330	0.077
Inferior frontal gyrus (FL_inf_fr)	**1.29 ± 0.08**	**0.067**	**1.81 ± 0.42**	**0.234**	**0.013**	**1.27 ± 0.10**	**0.069**	**1.59 ± 0.34**	**0.214**	**0.047**	**1.42 ± 0.13**	**0.092**	**2.22 ± 0.69**	**0.313**	**0.008**	1.41 ± 0.10	0.075	1.89 ± 0.51	0.268	0.064
Straight gyrus (FL_strai)	1.93 ± 0.14	0.073	2.18 ± 0.37	0.171	0.286	1.92 ± 0.16	0.084	2.08 ± 0.35	0.168	0.432	2.24 ± 0.20	0.092	2.72 ± 0.72	0.265	0.083	2.18 ± 0.24	0.110	2.59 ± 0.42	0.161	0.054
Anterior cingulate gyrus (G_cing_ant)	1.76 ± 0.09	0.052	2.06 ± 0.37	0.179	0.061	1.75 ± 0.13	0.075	1.94 ± 0.32	0.165	0.348	1.89 ± 0.09	0.049	2.37 ± 0.63	0.267	0.061	1.90 ± 0.19	0.100	2.18 ± 0.53	0.242	0.450
Anterior orbital gyrus (FL_OFC_AOG)	**1.41 ± 0.12**	**0.087**	**1.94 ± 0.47**	**0.230**	**0.013**	**1.38 ± 0.10**	**0.076**	**1.76 ± 0.42**	**0.238**	**0.033**	1.58 ± 0.18	0.117	2.33 ± 0.75	0.323	0.057	1.55 ± 0.15	0.100	2.04 ± 0.69	0.338	0.111
Medial orbital gyrus (FL_OFC_MOG)	**1.72 ± 0.11**	**0.062**	**2.07 ± 0.39**	**0.188**	**0.043**	**1.67 ± 0.12**	**0.072**	**1.96 ± 0.36**	**0.223**	**0.044**	2.11 ± 0.15	0.072	2.61 ± 0.57	0.220	0.061	2.05 ± 0.16	0.077	2.52 ± 0.55	0.218	0.065
Lateral orbital gyrus (FL_OFC_LOG)	**1.23 ± 0.09**	**0.076**	**1.66 ± 0.37**	**0.223**	**0.030**	1.20 ± 0.10	0.087	1.49 ± 0.43	0.289	0.074	1.39 ± 0.16	0.112	1.91 ± 0.56	0.294	0.076	1.36 ± 0.17	0.127	1.79 ± 0.80	0.444	0.192
Posterior orbital gyrus (FL_OFC_POG)	**1.61 ± 0.15**	**0.094**	**2.03 ± 0.45**	**0.223**	**0.013**	**1.62 ± 0.07**	**0.048**	**1.90 ± 0.36**	**0.189**	**0.040**	1.92 ± 0.24	0.125	2.46 ± 0.68	0.278	0.060	1.93 ± 0.08	0.041	2.29 ± 0.50	0.217	0.055
Anterior medial temporal gyrus (Ant_TL_med)	1.89 ± 0.27	0.144	2.01 ± 0.39	0.171	0.866	1.82 ± 0.16	0.090	1.92 ± 0.33	0.196	0.708	2.45 ± 0.15	0.062	2.58 ± 0.66	0.256	0.980	2.37 ± 0.39	0.163	2.37 ± 0.46	0.193	0.965
Anterior inferior lateral temporal gyrus (Ant_TL_inf_lat)	1.54 ± 0.23	0.150	1.77 ± 0.46	0.259	0.606	1.48 ± 0.19	0.130	1.66 ± 0.40	0.238	0.245	1.87 ± 0.23	0.126	2.25 ± 0.83	0.366	0.686	1.74 ± 0.13	0.074	2.00 ± 0.70	0.351	0.506
Parahippocampal and ambient gyrus (G_paraH_amb)	2.05 ± 0.25	0.123	2.13 ± 0.33	0.157	>0.999	1.99 ± 0.09	0.048	2.04 ± 0.35	0.173	0.965	2.48 ± 0.20	0.079	2.53 ± 0.60	0.238	0.923	2.37 ± 0.32	0.134	2.42 ± 0.60	0.250	0.974
Superior posterior temporal gyrus (G_sup_temp_post)	1.38 ± 0.10	0.072	1.47 ± 0.54	0.369	0.771	1.41 ± 0.11	0.081	1.32 ± 0.15	0.117	0.273	1.49 ± 0.09	0.063	1.40 ± 0.93	0.665	0.082	**1.52 ± 0.20**	**0.134**	**1.12 ± 0.21**	**0.189**	**0.008**
Middle and inferior temporal gyrus (G_tem_midin)	1.54 ± 0.11	0.078	1.81 ± 0.42	0.232	0.286	1.54 ± 0.09	0.089	1.64 ± 0.32	0.195	0.768	1.82 ± 0.13	0.073	2.17 ± 0.63	0.291	0.605	1.80 ± 0.15	0.085	1.88 ± 0.46	0.248	0.896
Fusiforme gyrus (G_fus)	1.84 ± 0.17	0.097	1.94 ± 0.27	0.139	0.748	1.83 ± 0.2	0.068	1.86 ± 0.32	0.171	0.889	2.04 ± 0.20	0.101	2.19 ± 0.40	0.185	0.586	2.07 ± 0.26	0.126	2.11 ± 0.55	0.258	0.914

(*continued on next page*)

Table 3 (*continued*)

Cortical region	Mean SUVr left ± SDwithout PVEC					Mean SUVr right ± SDwithout PVEC					Mean SUVr left ± SDwith PVEC					Mean SUVr right ± SDwith PVEC				
	HC	CoV_{HC}	nfv-PPA	CoV_{NV}	p_{Cor}-value	HC	CoV_{HC}	nfv-PPA	CoV_{NV}	p_{Cor}-value	HC	CoV_{HC}	nfv-PPA	CoV_{NV}	p_{Cor}-value	HC	CoV_{HC}	nfv-PPA	CoV_{NV}	p_{Cor}-value
Posterior temporal gyrus (Post_TL)	1.50 ± 0.07	0.048	1.57 ± 0.25	0.158	0.907	1.50 ± 0.07	0.050	1.48 ± 0.23	0.160	0.710	1.65 ± 0.13	0.081	1.70 ± 0.36	0.210	0.990	1.63 ± 0.13	0.077	1.53 ± 0.34	0.222	0.335
Superior anterior temporal gyrus (G_sup_temp_ant)	1.55 ± 0.11	0.075	1.49 ± 0.40	0.268	0.287	1.53 ± 0.11	0.072	1.44 ± 0.25	0.170	0.272	2.23 ± 0.22	0.097	1.93 ± 0.59	0.304	0.116	**2.22 ± 0.21**	**0.094**	**1.88 ± 0.39**	**0.210**	**0.048**
Parietal lobe (PL_rest)	1.33 ± 0.10	0.077	1.46 ± 0.32	0.219	0.730	1.34 ± 0.07	0.054	1.33 ± 0.25	0.194	0.670	1.54 ± 0.19	0.12	1.76 ± 0.49	0.279	0.546	1.56 ± 0.14	0.087	1.53 ± 0.40	0.263	0.526
Occipital lobe (OL_rest_lat)	1.24 ± 0.10	0.078	1.18 ± 0.19	0.164	0.363	1.24 ± 0.08	0.064	1.19 ± 0.24	0.205	0.233	1.32 ± 0.15	0.117	1.22 ± 0.27	0.222	0.300	1.31 ± 0.14	0.109	1.23 ± 0.34	0.280	0.161

3.2. Grey matter volume differences between patients with nfv-PPA and HC

Cortical grey matter volumes as assessed by individual T1-weighted MR images were significantly lower in nfvPPA patients, pronounced in the bilateral frontal cortex (left > right). The anterior inferior lateral temporal gyrus (bilateral) and the left parietal lobe also indicated significant grey matter volume loss after FDR-correction. Detailed grey matter volumes of all investigated cortical regions are provided in Table 2.

3.3. Impact of PVEC on quantitative [^{18}F]-THK-5351 uptake in patients with nfv-PPA and HC

When comparing the cortical [^{18}F]-THK-5351 uptake in uncorrected PET images between patients with nfv-PPA and healthy controls, bilateral frontal regions indicated a significantly elevated tracer signal (left > right). All single region comparisons are shown in Table 3 and group average images from patients with nfv-PPA and healthy controls are illustrated in Fig. 1.

After performing PVEC in all subjects, semi-quantitative differences between patients with nfv-PPA and HCs increased, especially in frontal cortical regions known to be affected in nfv-PPA. However, significant differences between nfv-PPA and HC were ameliorated in the contrast to uncorrected data (from 10 to 3 regions with significant difference) due to larger SUVr variations in both study groups after PVEC (Table 3). After PVE correction, the regional coefficients of variation (CoVs) increased in both groups and CoVs were higher in patients with nfv-PPA than in HCs (nfv-PPA uncorrected: 7.9 % ± 2.4 %, PVEC: 9.8 % ± 2.5 %; nfv-PPA uncorrected: 20.8 % ± 4.7 %, PVEC: 28.4 % ± 8.9 %). The only exception in the nfv-PPA patient group was the straight gyrus in the right hemisphere, which showed a CoV decrease. In HC, CoV decreased or remained at a similar level in five out of forty brain regions. Fig. 2 highlights cortical regions where PVEC increased the differences between patients with nfv-PPA and HCs in comparison to SUVr differences without PVEC. The highest impact of PVEC was observed in the bilateral motor cortex and the superior frontal gyrus (left > right).

All cortical regions with significantly SUVrs differences in nfv-PPA patients compared to HC after PVEC are shown in Table 3.

3.4. Effect of PVEC on the individual patient level

On a single patient level, patients with pronounced frontal cortical atrophy indicated stronger visual differences of cortical [^{18}F]-THK-5351 uptake after PVEC (Fig. 3).

Thus, we challenged this visual impression by a blinded visual read of three nuclear medicine physicians. Contrary to our expectations, sensitivity and specificity were 0.85/1.00 for uncorrected data, but a loss of specificity was observed for PVEC data (0.85/0.75). Interestingly, this result was obtained despite higher subjective reader confidence after PVE correction compared to uncorrected data ($p = 0.030$) (Fig. 4).

4. Discussion

The presented study shows manifold differences in the brains of nfv-PPA patients, when compared to healthy controls. Overall, the grey matter volume especially in the frontal lobe regions was significantly lower in nfv-PPA patients compared to the healthy control group, with an emphasis on the speech-dominant left hemisphere. The brain regions predominantly affected by cerebral atrophy in both brain hemispheres mainly distributed to the frontal lobe (superior frontal gyrus, straight gyrus, anterior cingulate gyrus and the regions of the fronto-orbital gyrus). Additional regions with significant volume reduction were on the left hemisphere the inferior frontal gyrus, the parietal lobe and the anterior inferior lateral temporal gyrus. These findings are consistent with prior imaging data showing similar results describing brain atrophy

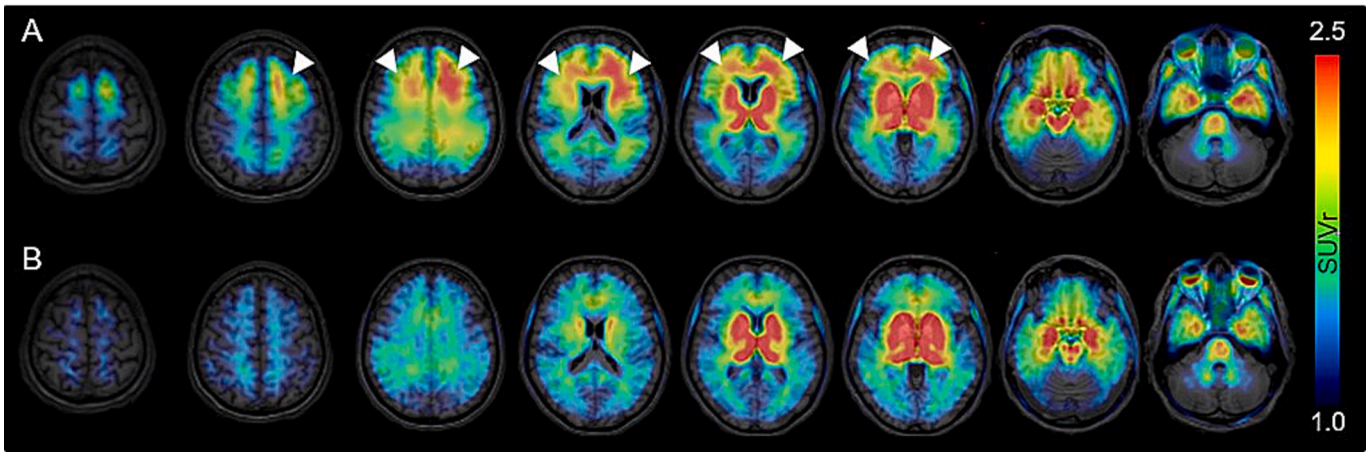

Fig. 1. Group average [^{18}F]-THK-5351 tracer uptake images without PVEC from (A) patients with nfv-PPA and (B) HC without PVEC. nfv-PPA = non-fluent/agrammatic primary progressive aphasia; HC = healthy control; SUVr = standard uptake value ratio, PVEC = partial volume effect correction.

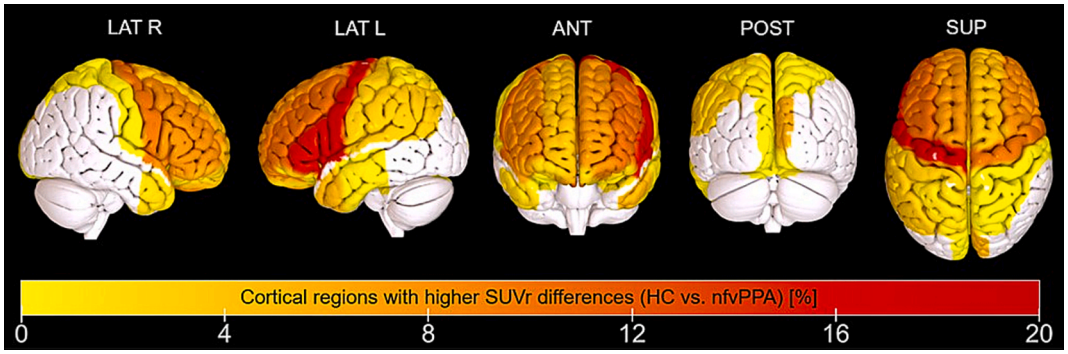

Fig. 2. Cortical regions with higher differences between HC and nfv-PPA patients before and after PVEC (difference of higher uptake in nfv-PPA compared to HC in %) in three-dimensional surface projections of the brain. nfv-PPA = non-fluent/agrammatic primary progressive aphasia; HC = healthy control; SUVr = standard uptake value ratio; LAT = lateral; ANT = anterior, POST = posterior; SUP = superior; R = right; L = left.

in the left inferior frontal gyrus, the orbitofrontal gyrus, and the lateral temporal gyrus (Josephs et al., 2006; Zhou et al., 2012; Brambati et al., 2015; Mandelli et al., 2016; Tetzloff et al., 2018).

This severe cerebral atrophy was accompanied by a significantly higher cortical [^{18}F]-THK-5351 tracer uptake prior to PVEC, indicating a higher abundance of tau and reactive inflammatory astrogliosis in the affected brain regions, which underlines the pathophysiological importance of these pathological hallmarks in nfv-PPA. For these regions the mean SUVr difference was increased by PVEC, but surprisingly, even though mean SUVr difference strongly increased for most of these regions, the significance levels decreased after PVEC. The lack of statistical significance in several regions after PVEC was caused by a higher variance among nfv-PPA patients and healthy controls in general, as shown by higher coefficients of variance in both groups.

The lacking value of PVEC was confirmed by a blinded visual read. The increase of SUVr in the affected brain regions had no impact on the sensitivity regarding the diagnosis of nfv-PPA, but the specificity dropped by 25 % meaning the tracer signal becomes stronger due to PVEC but less specific. Interestingly the left inferior frontal gyrus – a region regarded as the epicenter of tau pathology in nfv-PPA – remained significant after PVEC and the SUVr difference between healthy controls and nfv-PPA patients even further increased (Zhou et al., 2012; Mandelli et al., 2016). A possible explanation for this effect is a high signal spillover of [^{18}F]-THK-5351 signals from the epicenter region to the surrounding tissue. With PVEC this spill over is corrected and the SUVr increase is spatially more limited to epicenter region. Therefore, the surrounding tissue loses its [^{18}F]-THK-5351 signal intensity in some cases, which ultimately leads to a higher variance and loss of significance.

From a clinical perspective [^{18}F]-THK-5351-PET seems to be a reliable diagnostic tool to distinguish nfv-PPA patients from healthy controls with high sensitivity and specificity. In how far these results can be translated to distinguish nfv-PPA from other neurodegenerative dementias like bv-FTD, sv-PPA or AD remains unclear. Prior studies using [^{18}F]-THK-5351-PET in PPA patients of all three variants and healthy controls showed distinct binding patterns for each variant (Schaeverbeke et al., 2018). For an optimized diagnosis additional PET strategies might also be considered. The clinically most widespread approach is probably 2-Deoxy-2-[^{18}F]-Fluoro-D-Glucose PET-Imaging (FDG-PET). In various studies FDG-PET imaging demonstrated high discrimination rates between all three PPA-variants, other dementias and healthy controls (Mirbod et al., 2024; Matias-Guiu et al., 2022). Combinations of [^{18}F]-THK-5351-PET with FDG-PET in clinically uncertain cases would most likely improve the diagnostic quality.

Other PET-imaging strategies to detect activated microglia could also contribute to a more precise diagnosis of nfv-PPA patients, however next generation neuroinflammatory tracers like [^{18}F]-SMBT-1 and [^{18}F]-F-DED are not established yet (Lee et al., 2024; Ballweg et al., 2023). Furthermore, as nfv-PPA can also be caused by an AD-pathology a supplementary amyloid-PET-imaging using ^{18}F-florbetaben for example could give additional insights concerning the underlying pathology.

Besides the PET-imaging techniques the influence of different PVEC methods also needs to be considered. In our study we focused on the region-based voxel-wise PVEC method (RBV), however studies indicate, that other PVEC methods like Meltzer's or Mueller-Gaertner could have different results (Costoya-Sanchez et al., 2024; Greve et al., 2016).

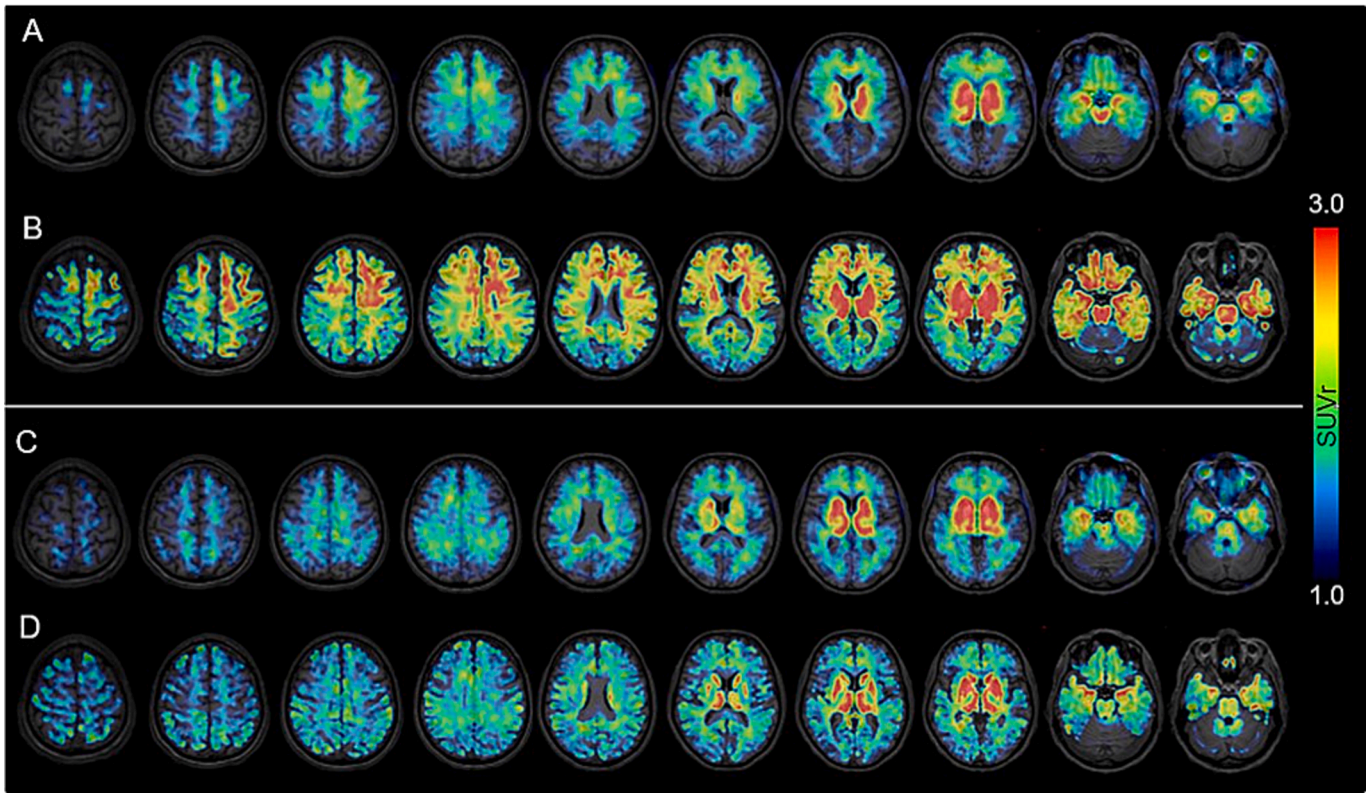

Fig. 3. Exemplary images of one nfv-PPA patient without/with PVEC (A, B) compared to one HC without/with PVEC (C, D). nfv-PPA = non-fluent/agrammatic primary progressive aphasia; HC = healthy control; SUVr = standard uptake value ratio, PVEC = partial volume effect correction.

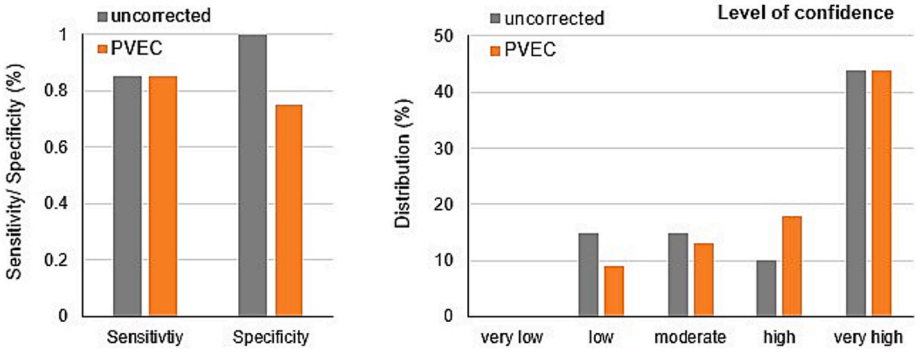

Fig. 4. Results of a blind visual read of [^{18}F]THK-5351 SUVr images with and without PVEC.

Further studies are required to clarify whether our results can be translated to other PVEC methods.

There are some limitations to our study. First, the used tracer – as other first-generation tracers – is not solely specific to tau and shows a relatively strong off target binding to astrogliosis-related MAO-B. Completely attributing all the signal intensity differences to the underlying proteinopathy is therefore not possible. [^{18}F]-THK-5351 SUVr differences are therefore very likely not only caused by the underlying proteinopathy, but also by differences in the reactive astrogliosis, what might be an additional contributor to [^{18}F]-THK-5351 SUVr variance. Second, even though our cohort is the largest nfv-PPA cohort examined using [^{18}F]-THK-5351, as nfv-PPA is a rather rare disease our sample size was limited to 20 patients. Further replications of our results with independent samples would therefore be recommended.

In conclusion our study shows significant differences of cerebral [^{18}F]-THK-5351 signals and distribution in nfv-PPA patients compared to healthy controls. Despite severe atrophy in patients with nfv-PPA, PVEC does not add any further value to the analysis of [^{18}F]-THK-5351 PET scans since the signal becomes less specific due to increasing signal variance.

Author contributions

The work was designed by MB, LB, TG and AR. Manuscript was written by PS and SS. PS, SS, OG, FMS, MS, FE, AK, MH, PB, TW and LW contributed to acquisition of data and/or analysis. Data and results were interpreted by PS, SS, NO, JP, AR, LB, TG and MB. PS, SS, LB, TG and MB drafted the work. NK, JP, AR, LB and AR substantively revised the work. All authors read and approved the final manuscript.

Funding.

Not project-related: LB was funded by the Munich-Clinician-Scientist-Program (LMU Munich).

CRediT authorship contribution statement

Patrick J. Sommer: Writing – original draft, Visualization, Formal analysis, Data curation. **Sebastian Schuster:** Writing – original draft, Formal analysis, Data curation. **Oliver Goldhardt:** Writing – review & editing, Methodology, Data curation. **Nobuyuki Okamura:** Writing – review & editing, Validation, Supervision, Project administration, Methodology, Investigation. **Felix Mueller-Sarnowski:** Writing – review & editing, Resources, Methodology, Investigation, Formal analysis. **Maximilian Scheifele:** Writing – review & editing, Resources, Investigation, Data curation. **Florian Eckenweber:** Writing – review & editing, Resources, Investigation, Data curation. **Annika Kreuzer:** Resources, Methodology, Investigation, Data curation. **Maria Griessl:** Writing – review & editing, Resources, Methodology, Investigation, Data curation. **Peter Bartenstein:** Writing – review & editing, Supervision, Resources, Investigation. **Thomas Wegehaupt:** Writing – review & editing, Investigation, Data curation. **Lucas Wolski:** Writing – review & editing, Methodology, Investigation, Data curation. **Josef Priller:** Writing – review & editing, Supervision, Resources, Methodology, Investigation. **Axel Rominger:** Writing – review & editing, Supervision, Resources, Project administration, Methodology, Investigation. **Leonie Beyer:** Visualization, Methodology, Investigation, Conceptualization. **Timo Grimmer:** Writing – review & editing, Supervision, Resources, Project administration, Methodology, Investigation, Data curation. **Matthias Brendel:** Writing – review & editing, Supervision, Resources, Project administration, Methodology, Investigation, Data curation, Conceptualization.

Declaration of competing interest

The authors declare the following financial interests/personal relationships which may be considered as potential competing interests: LB is a Novartis Pharma GmbH employee, unrelated to this work. Outside the submitted work TG reported receiving consulting fees from AbbVie, Alector, Anavex, Biogen, BMS; Cogthera, Eli Lilly, Functional Neuromodulation, Grifols, Iqvia, Janssen, Noselab, Novo Nordisk, NuiCare, Orphanzyme, Roche Diagnostics, Roche Pharma, UCB, and Vivoryon; lecture fees from Biogen, Eisai, Grifols, Medical Tribune, Novo Nordisk, Roche Pharma, Schwabe, and Synlab; and has received grants to his institution from Biogen, Eisai, and Roche Diagnostics. MB is a member of the Neuroimaging Committee of the EANM. MB received speaker honoraria from Roche, GE healthcare and Life Molecular Imaging and is an advisor of Life Molecular Imaging and MIAC. All other authors declare that the research was conducted in the absence of any commercial or financial relationships, that could be construed as a potential conflict of interest.

Acknowledgments

The authors thank the staff of the department of nuclear medicine at the University Hospital LMU Munich, the staff of the Centre for Cognitive Disorders at the Technical University Munich and especially the patients and their caregivers.

Data availability

Data will be made available on request.

References

Ballweg, A., Klaus, C., Vogler, L., Katzdobler, S., Wind, K., Zatcepin, A., et al., 2023. [18F]F-DED PET imaging of reactive astrogliosis in neurodegenerative diseases: preclinical proof of concept and first-in-human data. J. Neuroinflamm. 20, 68.

Benjamini, Y., Hochberg, Y., 1995. Controlling the false discovery rate: a practical and powerful approach to multiple testing. J. Royal Stat. Soc. Series B (Methodol.) 57, 289–300.

Brambati, S.M., Amici, S., Racine, C.A., Neuhaus, J., Miller, Z., Ogar, J., et al., 2015. Longitudinal gray matter contraction in three variants of primary progressive aphasia: A tenser-based morphometry study. Neuroimage Clin. 8, 345–355.

Brendel, M., Delker, A., Rötzer, C., Böning, G., Carlsen, J., Cyran, C., et al., 2014. Impact of partial volume effect correction on cerebral β-amyloid imaging in APP-Swe mice using [(18)F]-florbetaben PET. Neuroimage 84, 843–853.

Brendel, M., Högenauer, M., Delker, A., Sauerbeck, J., Bartenstein, P., Seibyl, J., et al., 2015. Improved longitudinal [(18)F]-AV45 amyloid PET by white matter reference and VOI-based partial volume effect correction. Neuroimage 108, 450–459.

Brendel, M., Reinisch, V., Kalinowski, E., Levin, J., Delker, A., Därr, S., et al., 2016. Hypometabolism in brain of cognitively normal patients with depressive symptoms is accompanied by atrophy-related partial volume effects. Curr. Alzheimer Res. 13.

Brendel, M., Wagner, L., Levin, J., Zach, C., Lindner, S., Bartenstein, P., et al., 2017. Perfusion-phase [18F]THK5351 Tau-PET imaging as a surrogate marker for neurodegeneration. J. Alzheimers Dis. Rep. 1, 109–113.

Brendel, M., Schönecker, S., Höglinger, G., et al., 2018. [18F]-THK5351 PET Correlates with topology and symptom severity in progressive supranuclear palsy. Front. Aging Neurosci. 9.

Cho, H., Kim, H.J., Choi, J.Y., Ryu, Y.H., Lee, M.S., Na, D.L., et al., 2019. 18 F-flortaucipir uptake patterns in clinical subtypes of primary progressive aphasia. Neurobiol. Aging 75, 187–197.

Costoya-Sanchez, A., Moscoso, A., Sobrino, T., Ruibal, Á., Grothe, M.J., Schöll, M., et al., 2024. Partial volume correction in longitudinal tau PET studies: is it really needed? Neuroimage 289.

Gorno-Tempini, M.L., Hillis, A.E., Weintraub, S., Kertesz, M.M., Cappa, S.F., et al., 2011. Classification of primary progressive aphasia and its variants. Neurology 76.

Greve, D.N., Salat, D.H., Bowen, S.L., Izquierdo-Garcia, D., Schultz, A.P., Catana, C., et al., 2016. Different partial volume correction methods lead to different conclusions: an 18F-FDG PET study of aging. Neuroimage 132, 334.

Harada, R., Ishiki, A., Kai, H., Sato, N., Furukawa, K., Furumoto, S., et al., 2018. Correlations of 18F-THK5351 PET with postmortem burden of tau and astrogliosis in Alzheimer disease. J. Nucl. Med. 59, 671–674.

Harris, J.M., Gall, C., Thompson, J.C., Richardson, A.M., Neary, D., du Plessis, D., et al., 2013. Classification and pathology of primary progressive aphasia. Neurology 81, 1832–1839.

Hodges, J.R., Davies, R.R., Xuereb, J.H., Casey, B., Broe, M., Bak, T.H., et al., 2004. Clinicopathological correlates in frontotemporal dementia. Ann. Neurol. 56, 399–406.

Josephs, K.A., Duffy, J.R., Strand, E.A., et al., 2006. Clinicopathological and imaging correlates of progressive aphasia and apraxia of speech. Brain 129, 1385–1398.

Josephs, K.A., Martin, P.R., Botha, H., Schwarz, C.G., Duffy, J.R., Clark, H.M., et al., 2018. [18 F]AV-1451 tau-PET and primary progressive aphasia. Ann. Neurol. 83, 599–611.

Lee, N., Choi, J.Y., Ryu, Y.H., 2024. The development status of PET radiotracers for evaluating neuroinflammation. Nucl. Med. Mol. Imaging 58, 160–176.

Lombardi, J., Mayer, B., Semler, E., Anderl-Straub, S., Uttner, I., Kassubek, J., et al., 2021. Quantifying progression in primary progressive aphasia with structural neuroimaging. Alzheimers Dement. 2021. https://doi.org/10.1002/ALZ.12323.

Mackenzie, I.R.A., Neumann, M., 2016. Molecular neuropathology of frontotemporal dementia: insights into disease mechanisms from postmortem studies. J. Neurochem. 138 (Suppl 1), 54–70.

Makaretz, S.J., Quimby, M., Collins, J., Makris, N., McGinnis, S., Schultz, A., et al., 2018. Flortaucipir tau PET imaging in semantic variant primary progressive aphasia. J. Neurol. Neurosurg. Psychiatry 89, 1024–1031.

Mandelli, M.L., Vilaplana, E., Brown, J.A., Hubbard, H.I., Binney, R.J., Attygalle, S., et al., 2016. Healthy brain connectivity predicts atrophy progression in non-fluent variant of primary progressive aphasia. Brain 139, 2778–2791.

Matias-Guiu, J.A., Suárez-Coalla, P., Yus, M., Pytel, V., Hernández-Lorenzo, L., Delgado-Alonso, C., et al., 2022. Identification of the main components of spontaneous speech in primary progressive aphasia and their neural underpinnings using multimodal MRI and FDG-PET imaging. Cortex 146, 141–160.

Mesulam, M.-M., Rogalski, E.J., Wieneke, C., Hurley, R.S., Geula, C., Bigio, E.H., et al., 2014. Primary progressive aphasia and the evolving neurology of the language network. Nat. Rev. Neurol. 10, 554–569.

Mesulam, M.-M., Weintraub, S., Rogalski, E.J., Wieneke, C., Geula, C., Bigio, E.H., 2014. Asymmetry and heterogeneity of Alzheimer's and frontotemporal pathology in primary progressive aphasia. Brain 137, 1176–1192.

Mirbod, M., Ayubcha, C., Redden, H.W.K., Teichner, E., Subtirelu, R.C., Patel, R., et al., 2024. FDG-PET in the diagnosis of primary progressive aphasia: a systematic review. Ann. Nucl. Med. 38, 673–687.

Ng, K.P., Pascoal, T.A., Mathotaarachchi, S., Therriault, J., Kang, M.S., Shin, M., et al., 2017. Monoamine oxidase B inhibitor, selegiline, reduces 18F-THK5351 uptake in the human brain. Alzheimers Res. Ther. 9, 25.

Oyama, S., Hosoi, A., Ibaraki, M., McGinnity, C.J., Matsubara, K., Watanuki, S., et al., 2020. Error propagation analysis of seven partial volume correction algorithms for [18 F]THK-5351 brain PET imaging. EJNMMI Phys. 7.

R Core Team, 2023. A Language and Environment for Statistical Computing. R Foundation for Statistical Computing, p. 2023.

Ruksenaite, J., Volkmer, A., Jiang, J., Johnson, J., Marshall, C.R., Warren, J.D., et al., 2021. Primary progressive aphasia: toward a pathophysiological synthesis. Curr. Neurol. Neurosci. Rep. 21.

Schaeverbeke, J., Evenepoel, C., Declercq, L., Gabel, S., Meersmans, K., Bruffaerts, R., et al., 2018. Distinct [18 F]THK5351 binding patterns in primary progressive aphasia variants. Eur. J. Nucl. Med. Mol. Imaging 45, 2342–2357.

Schönecker, S., Brendel, M., Palleis, C., Beyer, L., Höglinger, G.U., Schuh, E., et al., 2019. PET imaging of astrogliosis and Tau facilitates Diagnosis of Parkinsonian Syndromes. Front. Aging Neurosci. 11.
Schuster, S., Beyer, L., Palleis, C., Harris, S., Schmitt, J., Weidinger, E., et al., 2022. Impact of partial volume correction on [18F]GE-180 PET quantification in subcortical brain regions of patients with corticobasal syndrome. Brain Sci. 12.
Spinelli, E.G., Mandelli, M., Miller, Z.A., Santos-Santos, M.A., Wilson, S.M., Agosta, F., et al., 2017. Typical and atypical pathology in primary progressive aphasia variants. Ann. Neurol. 81.
Tetzloff, K.A., Duffy, J.R., Clark, H.M., Strand, E.A., Machulda, M.M., Schwarz, C.G., et al., 2018. Longitudinal structural and molecular neuroimaging in agrammatic primary progressive aphasia. Brain 141, 302–317.
Thomas, B.A., Erlandsson, K., Modat, M., Thurfjell, L., Vandenberghe, R., Ourselin, S., et al., 2011. The importance of appropriate partial volume correction for PET quantification in Alzheimer's disease. Eur. J. Nucl. Med. Mol. Imaging 38, 1104–1119.
Vermeiren, C., Motte, P., Viot, D., Mairet-Coello, G., Courade, J.P., Citron, M., et al., 2018. The tau positron-emission tomography tracer AV-1451 binds with similar affinities to tau fibrils and monoamine oxidases. Mov. Disord. 33.
Yoon, C.W., Jeong, H.J., Seo, S., Lee, S.Y., Suh, M.K., Heo, J.H., et al., 2018. 18 F-THK5351 PET imaging in nonfluent-agrammatic variant primary progressive aphasia. Dement. Neurocogn. Disord. 17, 110.
Zhou, J., Gennatas, E.D., Kramer, J.H., Miller, B.L., Seeley, W.W., 2012. Predicting regional neurodegeneration from the healthy brain functional connectome. Neuron 73, 1216–1227.